Oil & Gas Science and Technology – Rev. IFP Energies nouvelles **75**, 52 (2020)

https://doi.org/10.2516/ogst/2020048

Available online at:
ogst.ifpenergiesnouvelles.fr

REGULAR ARTICLE OPEN ACCESS

Investigation of acid pre-flushing and pH-sensitive microgel injection in fractured carbonate rocks for conformance control purposes

Alireza Teimouri, Saeid Sadeghnejad*, and Amir Hossein Saeedi Dehaghani

Department of Petroleum Engineering, Faculty of Chemical Engineering, Tarbiat Modares University, 14115-111 Tehran, Iran

Received: 8 March 2020 / Accepted: 8 June 2020

Abstract. Waterflooding in fractured reservoirs is a challenging task due to the presence of high conductive flow pathways such as fractures. Much of the injected water passes through fractures without sweeping the oil in the low permeable area, which results in an early breakthrough. Implementing deep conformance control techniques can be a remedy for this early water breakthrough. pH-sensitive microgel injection is a conformance control method in which the dependency of microgel viscosity to pH guarantees easy injection of these microgels into formations at low pH environments. Because of the geochemical reactions among rock minerals, microgels, and a pre-flushing acid, the microgel pH increases; therefore, these microgels swell and block high conductive fractures. In this study, a designed visual cell containing rock samples is implemented to observe rock–microgel interactions during a pH-sensitive microgel flooding into a fractured carbonate medium. First, the dependency of fracture aperture changes to the acid pre-flush flow rate is examined. Then, we investigate the effect of pH-sensitive microgel concentration on its resistance to block fractures during post-water flooding by studying the gel failure mechanisms (e.g., adhesive separation, cohesive failure). Finally, the effect of an initial aperture of fracture is examined on microgel washout when water injection is resumed. The results showed that both decreasing the acid flow rate and lowering the initial aperture could increase the rate of aperture changes. Moreover, the microgel solution with a concentration of 1 wt% showed the highest resistance (98.2 psi/ft) against post-water injection. Additionally, this microgel concentration had the highest permeability reduction factor. Meanwhile, the smaller initial aperture of fracture contributed to a higher microgel resistance.

1 Introduction

The complexity of fluid flow and heterogeneity of fractured reservoirs provide both opportunities and operational problems during oil production from these reservoirs. During waterflooding, the injected water rapidly flows through fractures and high permeable strata and breaks through in production wells. Thus, this early water breakthrough leaves a high residual oil saturation in low permeable areas (rock matrix) and reduces ultimate oil recovery [1–3]. One remedy to overcome this early water breakthrough problem is implementing gel treatment methods like preformed particle gels [4, 5], pH-sensitive microgels [6, 7], pH-insensitive polymeric solutions [8], or other smart polymers [9].

The conformance control by pH-sensitive microgels is a new technique that attracts new applications recently. pH-sensitive microgels are highly sensitive to pH and capable of holding significant volumes of water that significantly increases their viscosity [10]. The viscosity of these microgel solutions is very low at low pH; however, the viscosity rockets after a critical pH value. This effect is a significant feature of pH-sensitive microgels in applications like deep conformance control. Polyacrylic acids with different cross-linkers are a common form of molecular networks of pH-sensitive microgels [11]. Their apparent viscosity depends on pH, salinity, polymer concentration, cross-linker density, and shear rate [12, 13]. When the carboxylic groups are ionized in the polyacrylate network, the charged groups repel each other. This repulsion causes the polymer chains to stretch, resulting in the swelling of the microgel and increasing the viscosity. The term microgel is used for gel particles composed of crosslinked polymer chains that their size is in the range of 5–500 nm.

Figure 1 illustrates the concept of conformance control during a pH-sensitive microgel flooding process. During water injection in fractured reservoirs, water flows rapidly through fractures toward production wells (Fig. 1a). This causes early water breakthrough, which reduces the efficiency of the waterflooding process. As a result, much of oil in rock matrix remains intact. By injecting pH-sensitive microgels into the reservoir and blocking the fractures (Fig. 1b), the post injected water shifts toward lower permeable matrix areas. The oil in these areas is swept, and eventually, oil production increases. It was also recommended to

* Corresponding author: sadeghnejad@modares.ac.ir

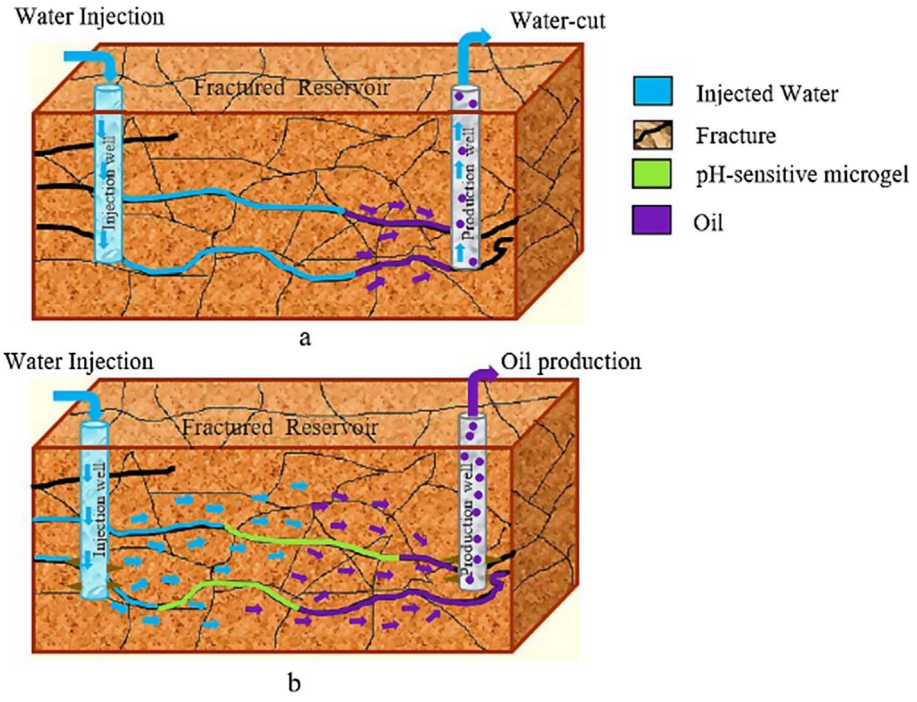

Fig. 1. The concept of deep conformance control in fractured reservoirs (a) an early breakthrough in fractured reservoirs during the waterflooding process due to the presence of high conductive fractures and (b) fracture plugging by pH-sensitive microgels and shifting the direction of the post injected water into the rock matrix and sweeping the remaining oil.

pre-flush the formation with acids before the main pH-sensitive polymer flooding [14]. Thus, microgels can keep their low viscosity at the new low-pH environment and are easily injected into the reservoir. This can guarantee the diffusion of gel polymers into deeper reservoir regions far from injection wells, which is known as the concept of deep conformance control. Using pH-sensitive microgels for conformance control applications is beneficial because of their availability, low cost, and environmentally friendly characteristics [15]. Moreover, unlike temperature-sensitive microgels, the process of microgel swelling, and blocking fractures is reversible. It means, if acid is injected into the reservoir, the microgel particles lose their swelling state, and blocked fractures can be reopened. This property is essential when fractures are required to be temporarily blocked.

On top of studying the chemical and rheological behavior of pH-sensitive microgels, some researchers investigated the injection of them into non-fractured sandstone and carbonate rocks. For example, Choi *et al.* examined geochemical reactions that cause pH alteration in sandstone both experimentally and by analyzing the results of a geochemical simulator, called KGEOFLOW. They found that geochemical reactions affect pH and ionic concentration of polymer solutions. Thus, considering these reactions is an essential step to model the behavior of pH-sensitive microgels in porous media [16]. Benson designed a hybrid simulator for injecting pH-sensitive microgels into sandstone rocks. They recommended that in reservoirs with a linear geometry, pH-sensitive slug injection has a better performance than continuous injection. Moreover, a weak acid pre-flush injection can improve the efficiency of conformance control [17]. Al-Wahaibi *et al.* examined various aspects of pH-sensitive microgel injection into sandstone rocks [18]. They showed that as the amount of the injected polymer increases, the surface of particles shows more resistance to the movement because of its particle sitting on the surface of the core, increasing a core pressure drop. Lalehrokh *et al.* were the pioneer of using pH-sensitive microgels in fractured reservoirs [7]. They injected these microgels into both sandstone and carbonate outcrop cores. For carbonates, the process of gelation was faster, and also the permeability reduction factor was higher. However, they did not discuss the primary mechanism of gel failure in fractures during post-water injection.

Generally, the rheological and chemical properties of pH-sensitive microgels and their viscosity behavior were mostly studied; however, the applicability of them in fractured reservoirs is not investigated in detail. Moreover, the main mechanisms of microgel failure in fractures were not also considered as well. Understanding the effect of these essential factors is crucial for fundamental conformance control studies in fractured reservoirs. In this study, we aim to investigate the acid pre-flush and pH-sensitive microgel injection into a fractured carbonate rock by a designed visual cell containing a real rock sample. This visual cell enables us to examine the acid–rock interactions in fractures by visual monitoring of the injected fluids. Moreover, the injection effect of an acid pre-flush on the geometrical properties of fractures (e.g., the rate of aperture changes) in carbonate reservoirs is investigated. Finally, the main mechanisms that affect microgel resistance to

block the fractures (failure mechanisms) during post-water injection are examined.

2 Materials and methods

2.1 Materials

2.1.1 Rock sample

The rock samples of this study are selected from the Sarvak formation of one of the Iranian central oil reservoirs. For measuring the rock properties, a 1.5-inch plug sample was drilled from the available 4-inch core sample. Subsequent to the Soxhlet cleaning, it was dried in an oven prior to any measurement. Then, the porosity and permeability of the sample were measured using the helium gas expansion method and the steady-state permeability measurement approach (*Petro Pajouhesh Ahoura Co.*), respectively. The porosity and permeability of the rock sample was 8% and 0.01 md, respectively. Table 1 shows the results of the X-Ray Fluorescence (XRF) test performed by an XRF PW2404 apparatus (UK) that determines the available minerals in the structure of the rock sample. As can be seen, the main composition of the rock sample is calcite.

Table 1. The results of XRF test showing the percent of existing minerals in the rock sample.

Mineral	Percentage (%)
L.O.I	41.540
CaO	54.867
MgO	1.510
Na_2O	0.063
Al_2O_3	0.607
SiO_2	0.359
P_2O_5	0.024
Cl	0.035
SO_3	0.026
Fe_2O_3	0.441
Ni	0.006
Sr	0.041
K_2O	0.028
TiO_2	0.19
MnO	0.036
Cu	0.046
Zr	0.011

2.1.2 Acid

According to the previous studies, weak acids have a better performance than strong acids in lowering a rock pH during an acid flooding process [14]. Thus, an acetic acid (*Merck, Germany*) was used in the acid pre-flushing experiments. Moreover, it was shown that the injection of acetic acid with a concentration higher than 13% causes precipitation and formation damage problems in carbonates [19]. Therefore, an 8 wt% solution of this acid was used during the experiments. This acid solution was stirred for an hour by a magnetic stirrer to complete the dissociation of ions in the water phase.

2.1.3 Polymer

A pH-sensitive polymer, called Carbopol®934 (*Lubrizol, USA*), was used in this study. This is a white, light, fluffy, and acidic powder with a density of 1.4 g/cm^3 and moisture content of 2.0%. Carbopol®934 is a polymer of acrylic acid. The used polymer powders had a diameter of about 0.2–6.0 micron, while the flocculated powders had a diameter of 2–7 micron (*Lubrizol, USA*). This polymer swells in water and some polar solvents producing viscous dispersions. Figure 2 illustrates the chemical structure of the Carbopol polymer used in this study.

To make the desired microgel solution, we added the polymer powder to distilled water gently to prevent polymer clogging. The polymer solution was stirred continuously for 24 h with a mechanical stirrer to yield a clear homogeneous solution. It is recommended to remove any air bubbles trapped in the polymer solution. For this purpose, a vacuum pump (*VE215, China*) was connected to the polymer solution container, and the polymer solution was vacuumed during stirring.

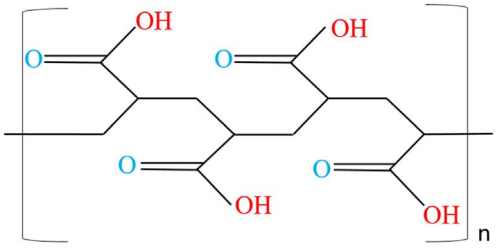

Fig. 2. The chemical structure of the carbopol polymer.

2.2 Flooding apparatus

Figure 3 illustrates the schematic of the flooding apparatus. This setup was designed in a way to analyze the behavior of pH-sensitive polymer injection in fractured carbonate rocks. This apparatus enables us to measure the pressure drop as well as visualize the flooding process by implementing a visual cell (No. 4 in Fig. 3). An HPLC pump (*Al-12-13, FLOM Co., Japan*, No. 1 in Fig. 3) and a transfer vessel (No. 2 in Fig. 3) were used to inject fluids into the visual cell. Moreover, microscopic images were taken from the fracture surface using a digital camera at different time intervals (No. 3 in Fig. 3). The time-lapse imaging data were analyzed to trace changes in the average fracture aperture. For monitoring the pressure drop of the flooding process, a differential pressure transmitter (*EJA130A, Yokogawa Co., Japan*) with the accuracy of 0.01 psi was used (No. 5 in Fig. 3). To vacuum the flooding system, we used a vacuum pump (*VE215, Younchi Co., China*) (No. 6 in Fig. 3). The pH of effluents was measured by a bench-top pH-meter (*edge®Hanna2020, Hanna Instruments, Italy*).

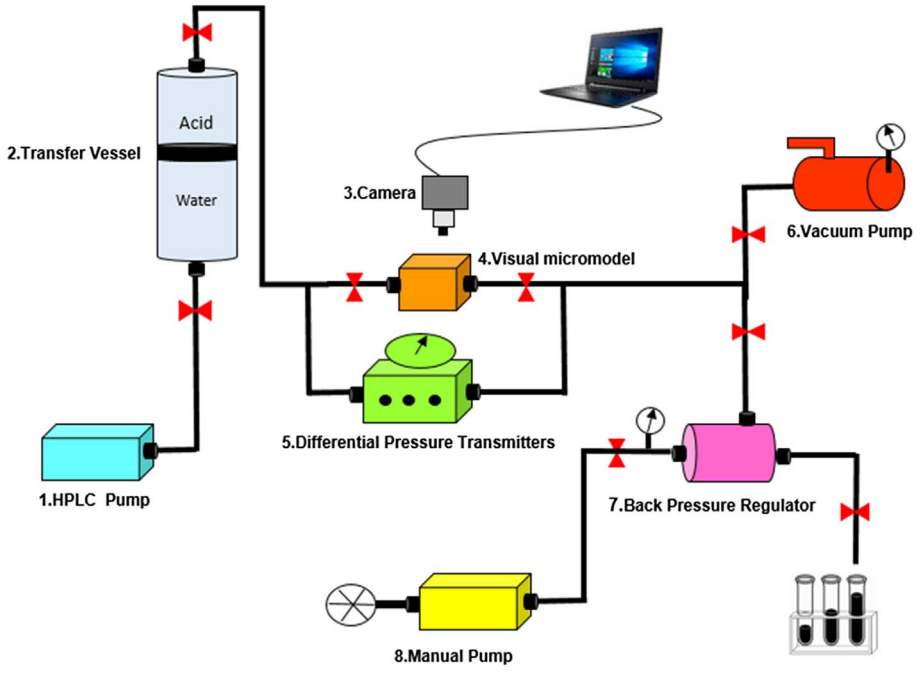

Fig. 3. Schematic of the flooding apparatus for acid pre-flushing analysis and plugging performance evaluation.

Based on the reaction of acetic acid with carbonate rocks, carbon dioxide gas is produced according to equation (1),

$$CaCO_3 + 2CH_3COOH \rightarrow Ca(CH3COO)_2 + H_2O + CO_2. \quad (1)$$

If the system pressure is kept high enough (above 85 psi), the produced gas remains dissolved into the aqueous phase [7, 20]. A 100 psi backpressure was applied to all experiments to prevent CO_2 from releasing. A back pressure regulator (*Petro-Ahoura Co., Iran*) was used to maintain the downstream pressure fixed (No. 7 in Fig. 3).

2.3 Visual cell

The cell of this study has two characteristics. First, it should enable us to work on a real rock sample for investigation of rock–polymer geochemical interactions. Thus, conventional glass micromodels cannot be used in this study. Second, it should provide a visual observation capability to monitor the behavior of microgel injection into fractured rocks. The designed and manufactured transparent cell is shown in Figure 4. It consists of two transparent Plexiglass plates (10 × 10 × 2 cm) used as the top and base of the cell (Nos. 7 and 2 in Fig. 4, respectively). A square pocket with a dimension of 6 × 6 × 0.8 cm was precisely machined at the center of the bottom plate to provide a holder for a slabbed rock to be installed in the cell (No. 2 in Fig. 4). Eight holes with a diameter of 0.8 cm were uniformly drilled across both upper and lower Plexiglass plates for inserting bolts and nuts. Bolts and nuts were used to stitch both plates together (Nos. 10 and 12 in Fig. 4). An opaque silicon rubber O-ring was used between the plates to prevent any fluid leakage during the experiments (No. 4 in Fig. 4). Another transparent PVC sealing rubber (No. 6 in Fig. 4) was installed between the rock sample (No. 5 in Fig. 4) in the cell and the upper plate of the Plexiglass plates (No. 7 in Fig. 4). This transparent sealing rubber enables us to access the rock faces for photography purposes. The designed cell was hydraulically tested up to 120 psi before the main experiments.

The calcite rock samples were carefully slabbed to be fixed into the rock holder. Considering the thickness of both PVC sealing at the top and bottom of the sample, 6 × 6 × 0.5 cm slabs of the rock samples were prepared. To create the fractures with the desired aperture, we used a fretsaw. Figure 4d depicts an installed rock sample into the visual cell.

2.4 Acid pre-flushing tests

Acid injection in fractured reservoirs can alter the fracture shapes (e.g., aperture), which affects the fracture permeability. To examine fracture aperture changes during the acid pre-flush experiments, we injected acetic acid into three identical rock samples with an initial fracture aperture of 0.5, 1.5, and 3.7 mm. In all experiments, after vacuuming, water injection was continued for 20 min with a low flow rate to ensure complete saturation. Then acetic acid was injected into the cell with two flow rates of 0.3 and 0.9 mL/min for 100 min. During the injection process, some images were taken from the rock at a 10-min time interval. Moreover, the effluents were collected in centrifuge tubes, and their pH value was measured. After finishing the experiments, the taken images were analyzed by IMAGE J software [21] to calculate the average fracture aperture changes during the acid flooding process. During the image analysis in IMAGE J software, the fracture length was divided into several equal intervals, and its aperture was measured at

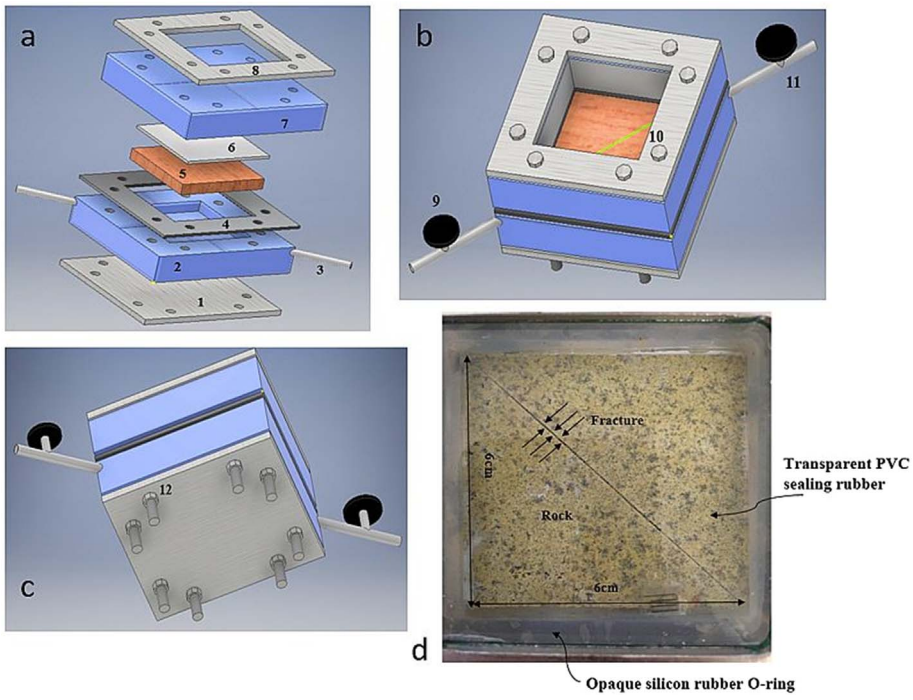

Fig. 4. Schematic of visual real-rock cell (a) different parts of cell, (b) side-view, (c) bottom-view of (a). The parts include (1) stainless steel shield, (2) lower Plexiglass plate, (3) stainless steel lines, (4) opaque silicon rubber O-ring, (5) carbonate rock, (6) transparent PVC sealing rubber, (7) upper Plexiglass plate, (8) stainless steel shield, (9) inlet valve, (10) bolts, (11) outlet valve, (12) nuts. (d) The created fracture inside the rock sample. The fracture aperture is shown with some arrows.

each point. Finally, the average aperture of the entire fracture was reported accordingly.

2.5 pH-sensitive microgel-plugging performance tests

One of the critical features of gel-based conformance control methods is the ability of injected gels to block fractures. If the blocking microgel has enough resistance to keep the fractures closed during the post-water injection, then the injected water cannot wash out the fracture gels. Then, it is forced to bypass fractures through the adjacent low permeable matrix zones. Thus, it can sweep the remaining oil and increase sweep efficiency. To study the microgel plugging performance, four microgel solutions with concentrations of 0.5, 1.0, 2.0, and 3.0 wt% were prepared and injected into fractured rocks with aperture sizes of 0.5, 1.5, and 3.7 mm.

After preparing the pH-sensitive microgel solution, it was injected into the cell to fill the entire space of the fracture. After that, the microgel remained in the fracture for a specific time (shut-in time). During this period, it reacted with rock minerals; therefore, the rock pH increased, and the particles swelled. The shut-in time for all experiments was 48 h. After the shut-in time, distilled water was pumped with a flow rate of 0.2 mL/min to evaluate the plugging efficiency of the microgels by monitoring the differential pressure across the cell. The index for measuring the microgel plugging performance is the maximum differential pressure that the gels can tolerate before being washed out. When the differential pressure suddenly drops, it shows that the microgel lost its resistance and water produced.

3 Results and discussion

3.1 Acid pre-flushing analysis

3.1.1 Effect of acid flow rate and fracture aperture

In this section, three rock samples with the initial fracture apertures of 0.5, 1.5, and 3.7 mm are used. In all samples first, an 8.0 wt% acetic acid solution was injected with a flow rate of 0.3 mL/min for 100 min. Then, the rock was cleaned by water injection for 10 min with the same rate, which is followed by another acetic acid injection with a flow rate of 0.9 mL/min. Table 2 summarizes the fracture initial pore volumes and porosity, and Figure 5 depicts the results of fracture aperture changes *versus* time for the three cases. As can be seen, by continuing the acid injection at both flow rates, the fracture aperture increases. The fracture aperture changes were calculated by analyzing the images taken during the injection process. The error bars in Figure 5 show the standard deviation of analysis for computing the fracture aperture at different points across the fracture length using the image processing software.

A criterion for the rate of reaction of the injected acid with the rock can be the slope of the graphs in Figure 5. The higher the slope, the faster the fracture aperture changes. Irrespective of the initial fracture aperture

Table 2. Initial pore volume and porosity of the three fractured models.

Fracture aperture (mm)	Fracture initial pore volume (mm^3)	Fracture porosity (%)
0.5	339.2	1
1.5	1017.6	3
3.7	2510.1	8

(compare Figs. 5a–5c), the slope of the injection flow rate of 0.3 mL/min is higher than that of 0.9 mL/min. During this low flow rate test, acetic acid had more time to be in contact with rock minerals at the surface of the fracture walls. In other words, it has a higher resident time. Thus, more minerals were dissolved in the injected acetic acid, and the variation of the fracture aperture was high. However, during the injection flow rate of 0.9 mL/min, the injected acetic acid left the fracture without any considerable reaction. For more investigation, the effluent pH *versus* time is plotted in Figure 6. Three distinct zones can be seen in this figure. Before the injection of acetic acid, the rock sample was saturated with water. During the acid injection, water inside of the fracture left the system (zone 1). The pH of the effluent decreases when acid breaks through. In zone 2, acetic acid continues to react with the surface of the fracture, slowly. In this area, the controlling factor is the competition between the injection rate and the acid–rock reaction rates. Over time, the injection from an unsteady state condition in zone 2 changes to a pseudo-steady-state condition in zone 3, in which the reaction reaches an equilibrium condition. While either the injection condition or the available minerals for reactions do not change, this pH remains in equilibrium. As indicated in Figure 6, the equilibrium effluent pH of the 0.3 mL/min flow rate for all three initial fracture apertures has a higher value than the 0.9 mL/min injection flow rate. For example, the equilibrium pH for the injection flow rate of 0.3 and 0.9 mL/min for the case with the initial aperture of 0.5 mm are 4.54 and 4.43, respectively. It can be concluded that when the flow rate is low, acetic acid could dissolve more amount of rock minerals; therefore, the outlet fluid contains less fresh acetic acid, and the effluent pH increased. Thus, lowering the injecting acid rates can speed up the fracture aperture changes.

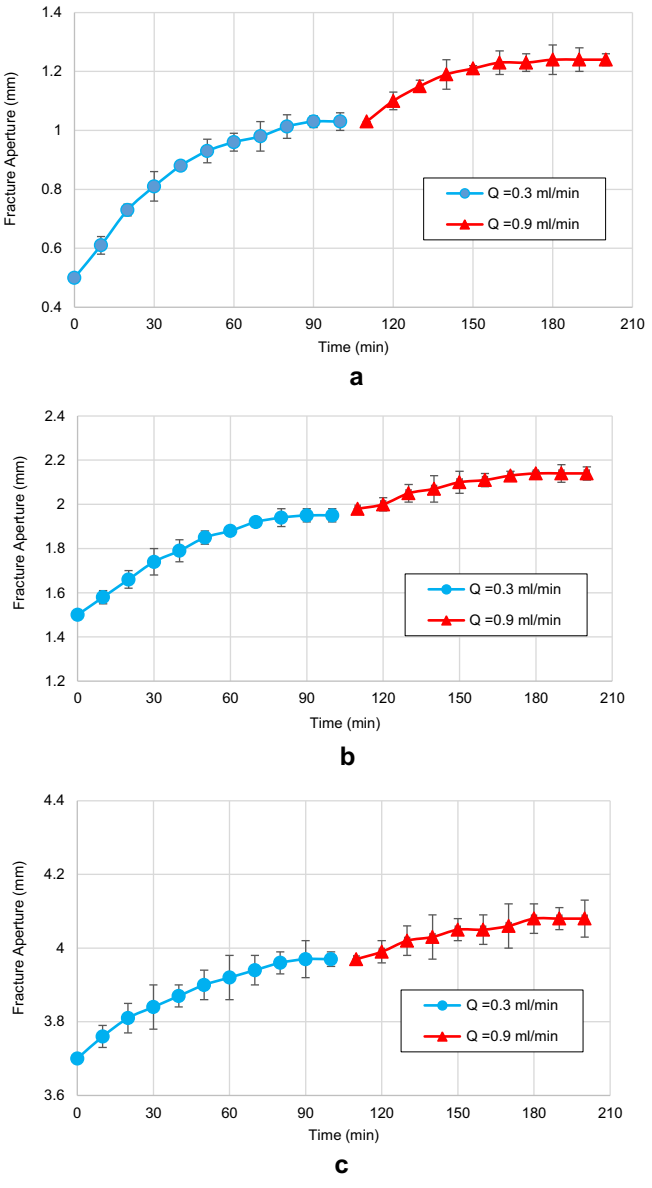

Fig. 5. The effect of acid injection flow rate on fracture aperture changes for the tests with an initial aperture of (a) 0.5 mm, (b) 1.5 mm, and (c) 3.7 mm.

3.1.2 Analyzing the rate of fracture aperture changes

The rate of fracture aperture changes in mm/min of all experiments was calculated from the first five data points of each graph of Figure 5; it is plotted in terms of the injection flow rate and initial fracture aperture in Figure 7. As can be seen, the rate of fracture aperture changes decreases when the initial fracture aperture rises. Besides, the tests with higher flow rates (0.9 mL/min) have a lower amount of aperture changes in comparison with those low injection flow rates (0.3 mL/min).

Three dimensionless numbers play a critical role in an acidizing process; Reynolds, Peclet, and Damkohler number. The Reynolds number (Re) determines the type of fluid flow regime (laminar or turbulent flow). In the study of fluid flow in fractures, this number is defined as [22, 23],

$$\mathrm{Re} = \frac{\rho v w}{\mu}, \tag{2}$$

where ρ is the fluid density (g/cm^3), v is the fluid velocity (cm/s), w and μ are the fracture aperture (cm) and fluid viscosity (g/cm s), respectively.

The Peclet number (pe) is another dimensionless number that is defined as the ratio of convection to diffusion rate [24],

$$\mathrm{pe} = \frac{v w}{24 D_e}, \tag{3}$$

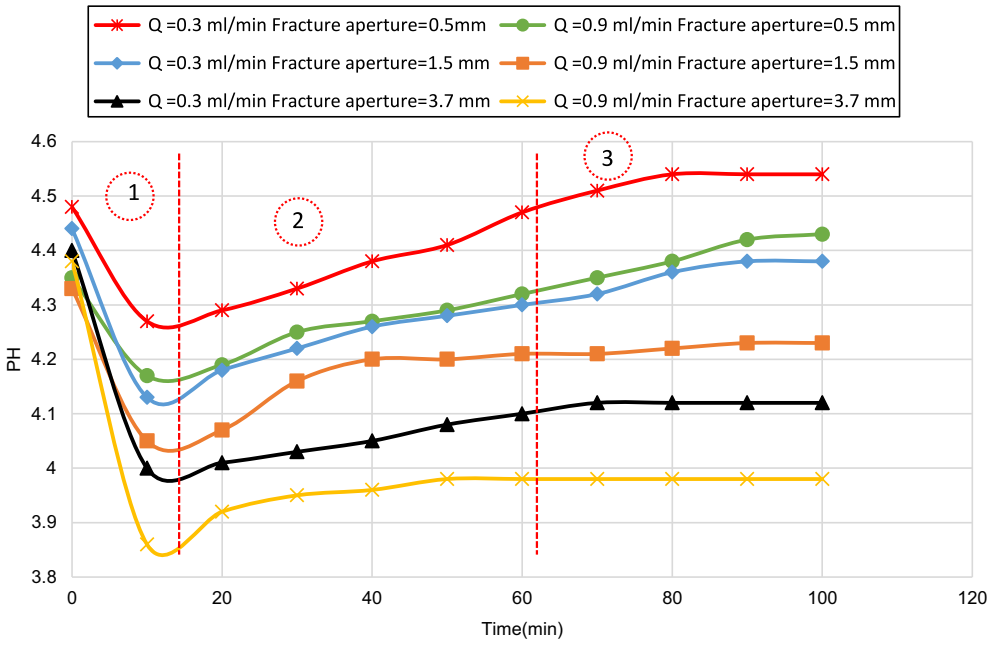

Fig. 6. The effluent pH during the injection of acetic acid.

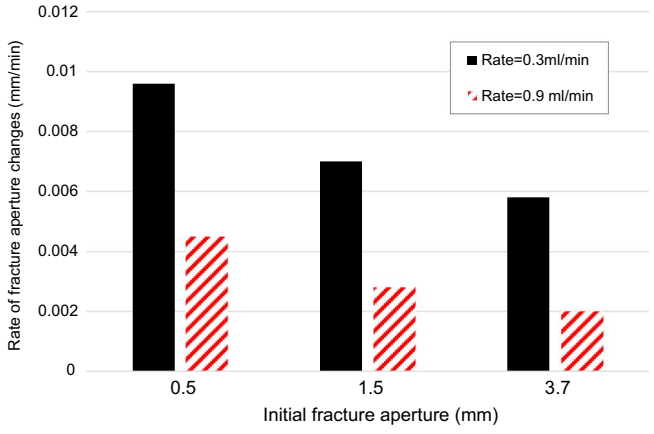

Fig. 7. Rate of fracture aperture increasing *versus* time for different initial fracture aperture sizes.

where D_e is the effective diffusion coefficient. Nierode [24] studied acid fracturing treatments and presented the values of the effective diffusive coefficient by,

$$D_e = (0.69 + (0.00293 \times \mathrm{Re} \times w)) \times 15.48384 \times 10^{-5} (\mathrm{cm}^2/\mathrm{s}). \quad (4)$$

The third number, which is the most important dimensionless number in the process of calcite dissolution in carbonate rocks, is the Damkohler number. This dimensionless number is defined as the ratio of the reaction to convection rate. Fredd and Fogler investigated wormhole formation in porous media by injection of strong acids, weak acids, and chelating agents [25]. They developed a comprehensive calcite dissolution model in which wormholes were considered similar to a capillary tube and proposed equation (5) for the calculation of the Damkohler number,

$$\mathrm{Da} = \frac{\pi d l \kappa}{Q}, \quad (5)$$

where κ,d, L, and Q are the dissolution rate constant (cm/s), the diameter of the capillary tube, the length of the capillary tube, and the flow rate (cm^3/s), respectively. Constant parameters used in these equations are listed in Table 3. Because of the geometry and size of the fractures in this study, we use the same equation (Eq. (5)) for calculation of the Damkohler number.

Fredd and Fogler suggested that the dissolution of calcite by acetic acid is influenced by the rate of transfer of reactants to calcite surface and rate of removal of products away from the rock surface [26]. Thus, it can be concluded that the surface reaction rate constant, the effective diffusivity of acid, and the injection rate are the most effective parameters during this process. However, the convection rate does not play any critical role [27]. If we multiply the Damkohler number by the Peclet number, the convection rate will be eliminated from the equations, and the mentioned effective parameters remain in the new dimensionless parameter,

$$\mathrm{Da} \times \mathrm{Pe} = \frac{\text{Convection}}{\text{Diffusion}} \times \frac{\text{Reaction}}{\text{Convection}} = \frac{\text{Reaction}}{\text{Diffusion}}. \quad (6)$$

For all acid pre-flush experiments (including both injections flow rates and the three fracture initial apertures), the Reynolds, Peclet, and Damkohler numbers are calculated and summarized in Table 4. It can be concluded that for a constant flow rate (tests 1–3 or 4–6 in Tab. 4), by increasing the initial fracture aperture, the product of Da × Pe rises as well. This parameter increases when either the

Table 3. Constant parameter used for analyzing the dimensionless numbers.

L (cm)	κ (cm/s)	μ (g/cm s)	ρ (g/cm^3)
8.48	1.4×10^{-4} [25]	0.01037 [31]	1.05 [31]

Table 4. Calculated Reynolds, Peclet, and Damkohler numbers for the experiments.

Test	Flow rate, Q (mL/min)	Fracture aperture (cm)	Velocity, v (cm/s)	Diffusion coefficient, D_e (cm^2/s) $\times 10^{-4}$	Re	Pe	Da	Da $\times$ Pe
1	0.3	0.05	0.1250	1.0685	0.632	2.437	0.037	0.090
2	0.3	0.15	0.0416	1.0688	0.631	2.432	0.111	0.269
3	0.3	0.37	0.0168	1.0694	0.629	2.421	0.275	0.665
4	0.9	0.05	0.3750	1.0688	1.898	7.309	0.012	0.087
5	0.9	0.15	0.1250	1.0696	1.898	7.304	0.037	0.270
6	0.9	0.37	0.0500	1.0715	1.873	7.193	0.091	0.654

reaction rate rises (the numerator of Eq. (6)) or the diffusion rate decreases (the denominator of Eq. (6)). Since the surface area of the fracture walls in contact with acid remains constant during the tests, the reaction rate does not change during the experiments. Therefore, the only remaining parameter that can control the fracture aperture is the diffusion rate, which is in agreement with the results of Fredd and Fogler [26]. Now we can explain the behavior of Figure 7, wherein the rate of fracture aperture increase was higher for the experiments with the smaller initial fracture apertures. When fracture aperture increases, more acetic acid enters into the fracture. However, to continue the dissolution process, this new acid needs time to diffuse near to the fracture surfaces and react with the calcite based on equation (1). To continue the reaction, the reaction products should diffuse back from the rock surface to the bulk of the fluid. As the reaction is diffusion dependent, more volume of acid remains unreacted and leaves the fracture when the fracture aperture increases (Fig. 8). This phenomenon can explain the behavior of Figure 6 as why the effluent pH decreases when the aperture increases at a constant injection rate.

3.2 pH-sensitive microgel injection

In the previous section, an acetic acid pre-flushing was studied to lower the rock environment pH before the main microgel injection. In this section, the main pH-sensitive microgel injection into the fractured rock is examined. The effect of two parameters, microgel concentration and the initial fracture aperture is analyzed. The efficiency of a deep conformance control technique is related to the fracture blocking capability of injected microgels. A successful microgel placement should have excellent resistance against washing out from fractures; therefore, the post-injected water can bypass fractures through adjacent matrix zones resulted in improving the efficiency of the water flooding process.

3.2.1 Microgel plugging performance

One of the parameters that have a significant impact on microgel resistance against washout is its concentration. Four different concentrations of the microgel (*i.e.*, 0.5, 1.0, 2.0, and 3.0 wt%) were injected into the fractured rock with an initial aperture of 0.5 mm, and their water plugging efficiency was analyzed. After 48 h of shut-in time, water was pumped into the fracture with a flow rate of 0.2 mL/min. The differential pressure across the fracture was monitored during this injection. The results of the plugging performance (the differential pressure across the fracture) of microgels with different concentrations are shown in Figure 9a. The plugging performance of a 3.0 wt% microgel was repeated twice to ensure the repeatability of the tests (Fig. 9b). The results show excellent reproducibility of the test results. For all experiments (except for 1.0 wt-%), by continuing water injection, the differential pressure across the fracture increases until a maximum value, wherein the microgels cannot keep the fracture closed, and the microgel breaks through by the injected water. This maximum pressure is called the microgel Holdback Pressure Gradient (HPG). In other words, the microgels begin to wash out at this peak point, and the differential pressure across the fracture suddenly decreases after that. However, the polymer concentration of 1.0 wt% showed a different behavior (Fig. 9a). In this test, the differential pressure went up until it reached roughly 20 psi after 100 min of water injection at a constant rate. At this point, the water started to be produced at a very low flow rate; however, the differential pressure did not drop suddenly, and the differential pressure remained constant between 20 and 22 psi (*i.e.*, point 1 in Fig. 9a). This observation indicates that there was a small leak in the microgel structure. However, the overall water plugging of the microgel was not wholly lost. Then, the injection flow rate was increased to 0.5 mL/min. During the next thirteen minutes, the differential pressure reached a stable value of approximately 22.8 psi (point 2 in

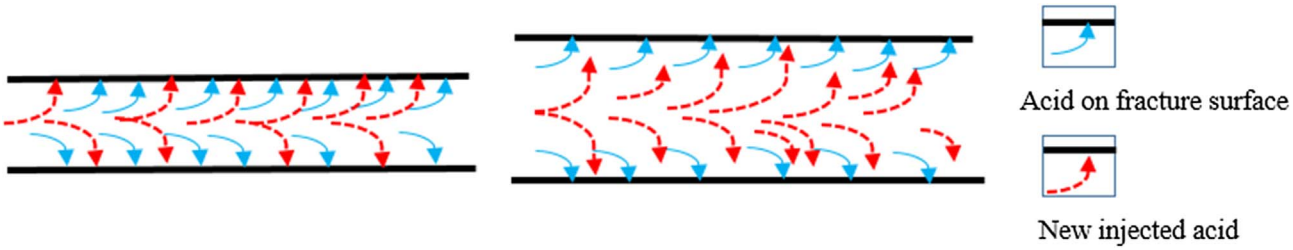

Fig. 8. The diffusion dependent mechanism of acetic acid injection into fractures with different apertures.

Fig. 9a). Finally, the flow rate increased to 1.0 mL/min, and a sudden decrease was observed at the differential pressure of 27.3 psi, and the microgel was expelled out of the model.

Figure 10 shows the microgel Holdback Pressure Gradient, HPG, (*i.e.*, the maximum differential pressure gradient recorded during post-water flooding in Fig. 9a) for different microgel concentrations. As can be seen, the microgels with the concentrations of 0.5 and 1.0 wt% have the minimum (33.4 psi/ft) and maximum (98.2 psi/ft) HPG among the studied concentrations. As observed, by increasing the microgel concentration (Fig. 10), the water plugging capability decreased. What is expected is that by increasing the microgel concentration, its viscoelastic properties and its HPG should be increased. However, an unexpected behavior was observed, which arises this question that why the microgel with a concentration of 1.0 wt% showed a better plugging performance than the other two higher concentrations (2.0 and 3.0 wt%)? This question will be answered in the subsequent chapter.

3.2.2 Gel failure mechanisms

Two main failure mechanisms are introduced in adhesive applications; adhesive separation, and cohesive failure [28]. In the adhesive separation mechanism (Fig. 11a), the separation of the adhesive gel from its substrate occurs by loss of the adhesive strength between the polymer and surface. While in the cohesive failure mechanism (Fig. 11b), the bulk gel breaks first. As an example, Figures 11c and 11d compare the expelled microgel of the visual cell for the concentrations of 3.0 and 1.0 wt%, respectively. Our visual investigations showed that during the post-water flooding with the 0.5 and 1.0 wt% microgel concentrations, the bulk microgel broke in a way that even at the end of the injection (after water breakthrough) a thin layer of gel remained sticking to the fracture surface (Fig. 11d). This shows that the failure mechanism was happened by the cohesive failure for these concentrations (Fig. 11b). On the contrary, during the post-water flooding with microgels of 2.0 and 3.0 wt% concentrations, a sudden decrease in the differential pressure across the fracture appeared, and the microgel was expelled out of the fracture in a bulk form (Fig. 11c). Thus, the failure mechanism in the polymer concentrations of 2.0 and 3.0 wt% should be the adhesive separation mechanism (Fig. 11a). This result shows that despite the higher strength of the bulk microgels at higher concentrations, the cohesion of them to the fracture surfaces was decreased by rising of the polymer concentration from 1.0 to 3.0 wt%. This change of the failure mechanism from cohesive failure to adhesion separation at the polymer concentration of 1.0 wt% can explain the behavior of the HPG of different microgel concentrations in Figure 10.

Gel strength is a function of its cross-linker density and is generally measured by its equilibrium modulus. By increasing the polymer solution concentration, the overall strength of the polymer bulk improves [10]. On the contrary, diluting a gel with a liquid can result in increasing the spacing between cross-linkers and softening the gel structure. This is why the gel with a concentration of 0.5 wt% showed a minimum HPG among the studied concentrations (Fig. 10). The microgel of this sample has the lowest concentration among the studied solutions; therefore, the bulk gel of this solution was not strong enough to resist the water breakthrough. Thus, the bulk gel cohesive failure mechanism occurs during the post-water flooding (Fig. 11b). However, the main question remained unanswered that why higher polymer concentrations (2.0 and 3.0 wt%) have a lower HPG than the 1.0 wt% concentration solution?

In the adhesion failure mechanism (the polymer solutions of 2.0 and 3.0 wt%), the adhesion of the gel to calcite surface in the fracture surface plays an essential role during plugging behavior studies (Fig. 11a). The adhesion of the polymer to its substrate is highly influenced by the polymer viscoelasticity and surface properties (*i.e.*, gel polymer wetting and its penetration into the surface roughness) [29]. To function correctly, polymeric adhesives must combine liquid-like characteristics to form good molecular contact and solid-like characteristics to resist applied stress once the gel has been formed [30]. The increase of the cross-link density increases polymer gel modulus [28]. By increasing the elastic moduli from 2.0 to 3.0 wt%, the bulk polymer behaves much stronger. However, the polymer adhesion characteristics decrease because the gel polymer is unable to dissipate energy via viscous contributions, or it cannot deform to maintain its contact with its substrate [30]. Thus, the inability to conform to the surface results in a weak gel-calcite adhesive contact [30]. As a result, at higher polymer concentrations, the gel modulus is higher than the interfacial strength of gel–calcite; consequently, the gel leaves the fracture with less residue on the calcite surface that will be discussed in the next section. These two phenomena can explain why by increasing the polymer concentration from 1.0 to 3.0 wt%, the HPG decreases (Fig. 10).

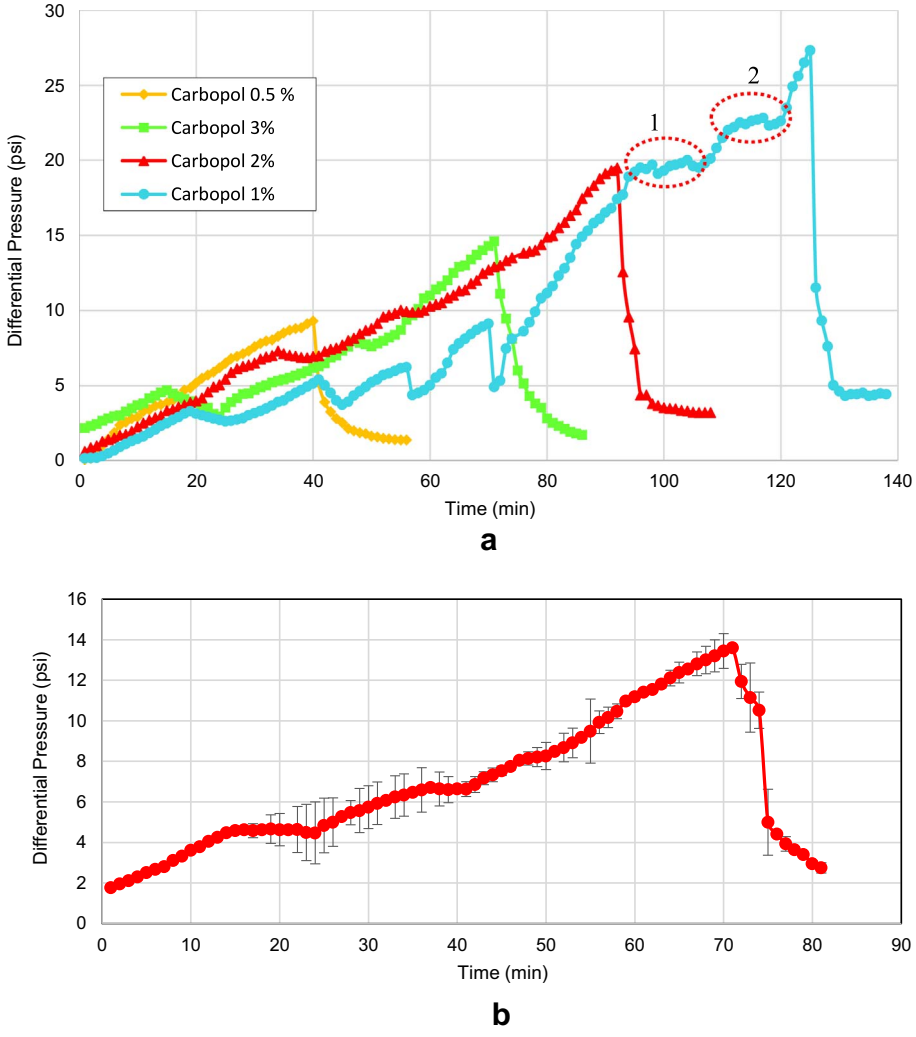

Fig. 9. (a) Fracture differential pressure during post-water flooding showing the microgel breakthrough pressure for different polymer concentrations. (b) Checking the repeatability of the microgel plugging performance test. The polymer concentration is 3.0 wt%.

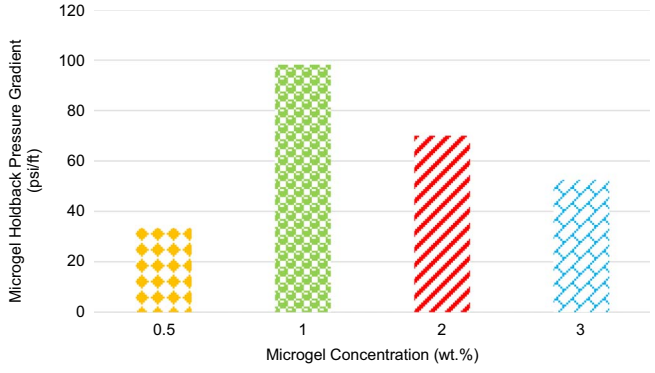

Fig. 10. Microgel Holdback Pressure Gradient (HPG) at different micro polymer concentrations.

During the gelation process, the gelant wetting and penetration into the surface roughness of the substrate are also two other important factors that affect the adhesive strength of the final gel. A perfect adhesive bond formation requires a high polymer segmental mobility at the molecular scale. During the gelation phase, the amount of contact between the gel and surface increases with the contact time by wetting of the surface and deformation of the polymer to accommodate surface roughness [30]. By increasing the polymer concentration, the spacing between cross-linkers reduces. Thus, the crosslinks try to adsorb polymer chains into the bulk gel. By decreasing the spacing between cross-linkers, the diffusion rate of polymer chains reduces as well. Less movability of polymer chains during the gelation phase prevents complete penetrating of them into the roughness of the fracture surface. Thus, the final gel is quickly be expelled out of the fracture with a lower amount of applied stress despite its higher bulk modulus. Considering both gel wetting ability and its amount of penetration into the surface roughness during the gelation phase reveals that by increasing the polymer concentration form 1.0 to 3.0 wt%, the gel adhesion to the calcite surface should decrease, which resulted in reducing of the HPG (Fig. 10).

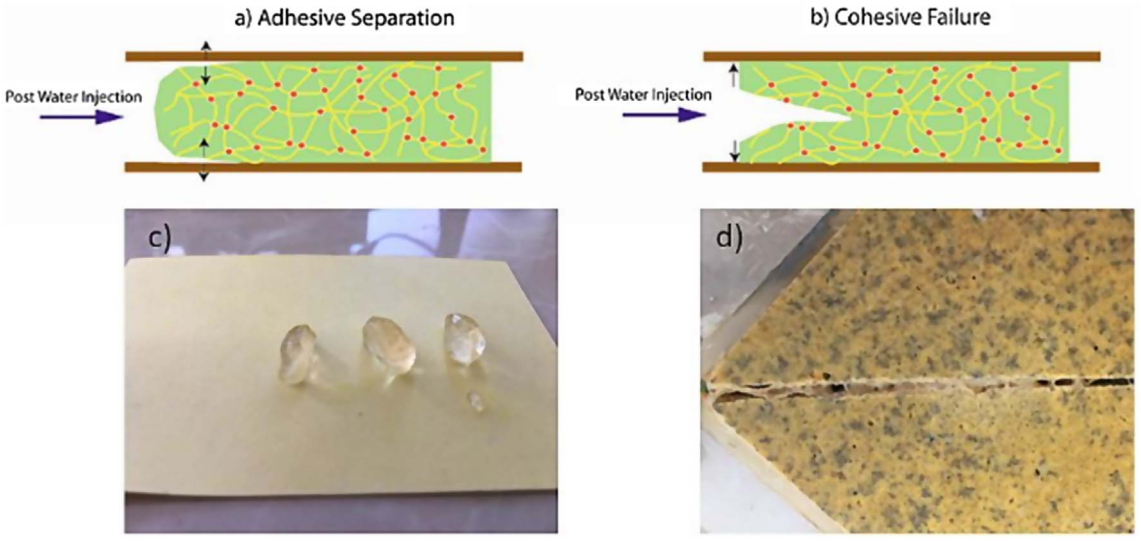

Fig. 11. Gel failure mechanisms, (a) adhesive separation, (b) cohesive failure, c) the bulk microgel with the concentration of 3.0 wt% expelled out from the fracture after microgel breakthrough, and (d) the formed microgel layer in the fracture aperture during post-water flooding into the fracture-filled with the microgel with a concentration of 1.0 wt%.

3.2.3 Permeability reduction factor analysis

Permeability Reduction Factor (PRF) is one of the main factors of understanding the efficiency of microgel capability for plugging the fracture. When water breaks through the microgel, the overall coherency of microgel is lost. PRF shows what percentage of the fracture permeability is lost due to the injection of the pH-sensitive microgel. By dividing the pressure drop after microgel breaking through to that before the microgel injection, the RPF can be calculated (Eq. (7)).

$$\mathrm{PRF} = \frac{\mathrm{DP}_A}{\mathrm{DP}_B}, \tag{7}$$

where DP_A and DP_B are pressure drop after and before microgel injection, respectively.

Table 5 compares the PRF value of the fractures with an initial aperture of 0.5 mm for different polymer concentrations. As indicated, the microgel with a concentration of 1.0 wt% had the maximum PRF among all cases. This shows that after the microgel breakthrough, a higher amount of the microgels remained in the fracture attached to its wall surfaces, which resulted in lowering the permeability of the system. Furthermore, as microgel concentration increases from 1.0 to 3.0 wt%, the PRF value decreases. It shows that the gels at the higher concentrations left the fracture with less residue on the fracture surface. It again demonstrates that by increasing the gel polymer concentration, its adhesive bonding to the calcite rock surface decreases.

Table 5. The PRF of the fracture sample with initial aperture of 0.5 mm.

Microgel concentration (wt%)	Differential pressure before microgel injection (psi)	Differential pressure after microgel breakthrough pressure (psi)	PRF
0.5	0.07	1.37	19.57
1.0	0.07	4.41	63
2.0	0.07	3.18	45.42
3.0	0.07	1.8	25.71

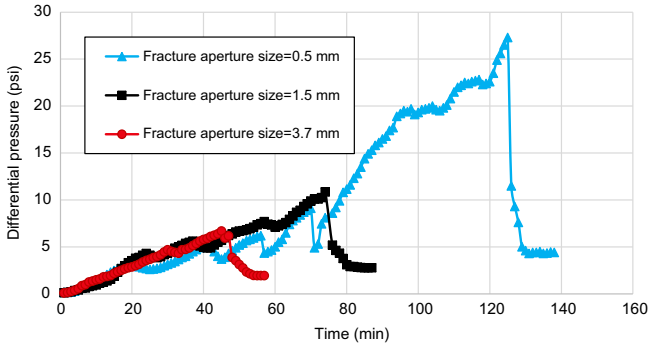

Fig. 12. Effect of initial fracture aperture on microgel plugging performance.

3.2.4 Effect of fracture aperture on microgel plugging performance

The initial fracture aperture can affect microgel-plugging behaviors. To examine this factor, we injected the microgel solution with the maximum water-plugging capability (1.0 wt%) into three fractures with the initial apertures of 0.5, 1.5, and 3.7 mm. After the 48 h of shut-in time, water was injected into the cell, and the plugging performance of these scenarios was examined (Fig. 12). As can be seen from Figure 12, the lower the initial fracture aperture, the higher

the water plugging performance is. In all fracture apertures, both the fracture surface area that microgels stick to it and the microgel concentration were constant. Therefore, the cohesion forces in all three cases are approximately equal. However, by increasing the initial fracture aperture, more volume of microgel was placed into the fracture volume, which led to lower microgel compaction. This causes a reduction in microgel plugging performances.

4 Conclusion

The purpose of this research was to investigate the process of deep conformance control of pH-sensitive microgels in fractured carbonate reservoirs. The study was consisted of analyzing acid pre-flushing and injection of pH-sensitive microgels into the fractured medium to investigate microgel plugging efficiency. A visual cell containing a real rock was implemented in a way that not only the interaction of rock–acid could be observed during acid injection, but also it could endure enough pressure for preventing carbon dioxide release.

The results of acid pre-flush showed that lowering the injection acid rate speeded up the rate of fracture aperture changes. According to the Damkohler and Peclet number analysis, it was revealed that the reaction of acetic acid with the calcite mineral was diffusion dependent. The higher the aperture size, the slower the rate of transfer of acid from the bulk of fluid into the fracture wall was. Thus, there was no enough time for the new acid to reach the fracture walls and react with it. Therefore, the rate of aperture changes decreased for those fractures with higher initial aperture. During the pH-sensitive microgel flooding experiments, it was revealed that these microgels could efficiently plug the fractures and push water into the matrix of the rock. This can increase the sweep efficiency of a reservoir during a water flooding process. It was revealed that there is an optimal concentration for the plugging performance of microgels. By increasing the gel polymer concentration, the gel failure mechanism changes from the cohesive failure to the adhesive separation. It means that high microgel concentrations are not always recommended as they have a lower coherency to fracture walls during the post-water flooding experiments. The microgel with a concentration of 1.0 wt% showed the highest plugging performance against the injected water. After microgel breakthrough, a maximum PRF was observed for this microgel as well. Further analyses also showed that the microgel breakthrough pressure decreased when the fracture aperture increased.

Acknowledgments. The authors would like to Dr. Somayeh Ghasemirad for discussions on gel polymer failure mechanisms.

References

1 Sadeghnejad S., Masihi M. (2011) water flooding performance evaluation using percolation theory, *J. Pet. Sci. Technol.* **1**, 2, 19–23.
2 de Aguiar K.L.N.P., de Oliveira P.F., Mansur C.R.E. (2020) A comprehensive review of in situ polymer hydrogels for conformance control of oil reservoirs, *Oil Gas Sci. Technol. - Rev. IFP Energies nouvelles* **75**, 1, 8.
3 Liu Y., Bai B., Wang Y. (2010) Applied technologies and prospects of conformance control treatments in China, *Oil Gas Sci. Technol. - Rev. IFP Energies nouvelles* **65**, 6, 859–878.
4 Bai B., Wei M., Liu Y. (2012) Injecting large volumes of preformed particle gel for water conformance control, *Oil Gas Sci. Technol. - Rev. IFP Energies nouvelles* **67**, 6, 941–952.
5 Yu L., Sang Q., Dong M. (2018) Enhanced oil recovery ability of branched preformed particle gel in heterogeneous reservoirs, *Oil Gas Sci. Technol. - Rev. IFP Energies nouvelles* **73**, 65.
6 Lalehrokh F. (2010) Applicability of pH-triggered polymers to increase sweep efficiency in fractured reservoirs, *PhD Thesis*, The University of Texas, Austin, 132 p.
7 Lalehrokh F., Bryant S.L., Huh C., Sharma M.M. (2008) Application of pH-triggered polymers in fractured reservoirs to increase sweep efficiency, in: *SPE Symposium on Improved Oil Recovery*, Society of Petroleum Engineers, Tulsa, USA.
8 Panthi K., Mohanty K.K. (2018) pH-insensitive polymeric particles for enhanced oil recovery in reservoirs with fractures, *SPE J.* **23**, 1, 34–47.
9 Ashrafizadeh M., Ahmad Ramazani S.A., Sadeghnejad S. (2017) Enhanced polymer flooding using a novel nano-scale smart polymer: Experimental investigation, *Can. J. Chem. Eng.* **95**, 11, 2168–2175.
10 Al-Anazi H.A., Sharma M.M. (2002) Use of a pH sensitive polymer for conformance control, in: *International Symposium and Exhibition on Formation Damage Control*, Society of Petroleum Engineers, Lafayette, USA.
11 Ashrafizadeh M., Tam K.C., Javadi A., Abdollahi M., Sadeghnejad S., Bahramian A. (2019) Synthesis and physicochemical properties of dual-responsive acrylic acid/butyl acrylate crosslinked nanogel systems, *J. Colloid Interface Sci.* **556**, 313–323.
12 Abdel-Goad M., Al-Wahaibi Y., Al-Wahaib T., Al-Shurji H. (2012) Use of a novel pH-triggered polymer-gel system for optimal mobility-control applications, *e-Polymers* **12**, 1.
13 Huh C., Choi S.K., Sharma M.M. (2005) Rheological model for pH-sensitive ionic polymer solutions for optimal mobility control applications, in: *SPE Annual Technical Conference and Exhibition*, Society of Petroleum Engineers, Dallas, USA.
14 Younesian-Farid H., Sadeghnejad S. (2019) Geochemical performance evaluation of pre-flushing of weak and strong acids during pH-triggered polymer flooding, *J. Pet. Sci. Eng.* **174**, 1022–1033.
15 Tavassoli S., Ho J.F., Shafiei M., Huh C., Bommer P., Bryant S., Balhoff M.T. (2018) An experimental and numerical study of wellbore leakage mitigation using pH-triggered polymer gelant, *Fuel* **217**, 444–457.
16 Suk K.C., Ermel Y.M., Bryant S.L., Huh C., Sharma M.M. (2006) Transport of a pH-sensitive polymer in porous media for novel mobility-control applications, in: *SPE/DOE Symposium on Improved Oil Recovery*, Society of Petroleum Engineers, Tulsa, USA.
17 Benson I.P. (2007) Numerical simulation of ph-sensitive polymer injection as a conformance control method, *Master of Science Thesis*, The university of Texas, Austin. 211 p.
18 Al-Wahaibi Y., Al-Wahaibi T., Abdelgoad M. (2011) Characterization of pH-sensitive Polymer microgel transport in porous media for improving oil recovery, *Energy Sources Part A Recovery Utilization Env. Effects* **33**, 11, 1048–1057.

19 Al-Khaldi M.H., Nasr-El-Din H.A., Mehta S., Al-Aamri A. (2007) Reaction of citric acid with calcite, *Chem. Eng. Sci.* **62**, 21, 5880–5896.
20 Choi S.K. (2005) A study of a pH-sensitive polymer for novel conformance control applications, *Master of Science Thesis*, The University of Texas, Austin, 162 p.
21 Schneider C.A., Rasband W.S., Eliceiri K.W. (2012) NIH Image to ImageJ: 25 years of image analysis, *Nat. Methods* **9**, 7, 671.
22 Javadi M., Sharifzadeh M., Shahriar K., Mitani Y. (2014) Critical Reynolds number for nonlinear flow through rough-walled fractures: The role of shear processes, *Water Resour. Res.* **50**, 2, 1789–1804.
23 Sarkar S., Toksoz M.N., Burns D.R. (2004) *Fluid flow modeling in fractures*, Massachusetts Institute of Technology. Earth Resources Laboratory, Cambridge, MA, USA.
24 Nierode D.E., Williams B., Bombardieri C. (1972) Prediction of stimulation from acid fracturing treatments, *J. Can. Pet. Technol.* **11**, 4, 31–41.
25 Fredd C.N., Fogler H.S. (1998) Influence of transport and reaction on wormhole formation in porous media, *AIChE J.* **44**, 9, 1933–1949.
26 Fredd C.N., Fogler H.S. (1998) The kinetics of calcite dissolution in acetic acid solutions, *Chem. Eng. Sci.* **53**, 22, 3863–3874.
27 Fredd C., Miller M. (2000) Validation of carbonate matrix stimulation models, in: *SPE International Symposium on Formation Damage Control*, Society of Petroleum Engineers, Lafayette, USA.
28 Shen J., Lin X., Liu J., Li X. (2018) Effects of crosslink density and distribution on static and dynamic properties of chemically crosslinked polymers, *Macromolecules* **52**, 1, 121–134.
29 Zosel A. (1989) Adhesive failure and deformation behaviour of polymers, *J. Adhes.* **30**, 1–4, 135–149.
30 Grillet A.M., Wyatt N.B., Gloe L.M. (2012) Polymer gel rheology and adhesion, *Rheology* **3**, 59–80.
31 Dai L.-Y., He D., Lei M., Chen Y. (2008) Densities and viscosities of binary mixtures of acetic acid with acetic anhydride and methenamine at different temperatures, *J. Chem. Eng. Data* **53**, 12, 2892–2896.